



저작자표시-비영리-변경금지 2.0 대한민국

이용자는 아래의 조건을 따르는 경우에 한하여 자유롭게

- 이 저작물을 복제, 배포, 전송, 전시, 공연 및 방송할 수 있습니다.

다음과 같은 조건을 따라야 합니다:



저작자표시. 귀하는 원저작자를 표시하여야 합니다.



비영리. 귀하는 이 저작물을 영리 목적으로 이용할 수 없습니다.



변경금지. 귀하는 이 저작물을 개작, 변형 또는 가공할 수 없습니다.

- 귀하는, 이 저작물의 재이용이나 배포의 경우, 이 저작물에 적용된 이용허락조건을 명확하게 나타내어야 합니다.
- 저작권자로부터 별도의 허가를 받으면 이러한 조건들은 적용되지 않습니다.

저작권법에 따른 이용자의 권리는 위의 내용에 의하여 영향을 받지 않습니다.

이것은 [이용허락규약\(Legal Code\)](#)을 이해하기 쉽게 요약한 것입니다.

[Disclaimer](#)

Master's Thesis

석사 학위논문

Synthesis and Characterization of Type II core/shell Nanocrystals for Quantum-Dot- Sensitized Solar Cells

Soo Jin Kim (김 수 진 金 秀 眞)

Department of Energy Systems Engineering

에너지시스템공학전공

DGIST

2015

Master's Thesis

석사 학위논문

Synthesis and Characterization of Type II core/shell Nanocrystals for Quantum-Dot- Sensitized Solar Cells

Soo Jin Kim (김 수 진 金 秀 眞)

Department of Energy Systems Engineering

에너지시스템공학전공

DGIST

2015

Synthesis and Characterization of Type II core/shell Nanocrystals for Quantum-Dot-Sensitized Solar Cells

Advisor : Professor Jong-Soo Lee

Co-Advisor : Professor Nak Cheon Jeong

By

Soo Jin Kim

Department of Energy Systems Engineering

DGIST

A thesis submitted to the faculty of DGIST in partial fulfillment of the requirements for the degree of Master of Science in the Department of Energy Systems Engineering. The study was conducted in accordance with Code of Research Ethics¹.

04.12. 2014

Approved by

Professor Jong-Soo Lee (Signature)

(Advisor)

Professor Nak Cheon Jeong (Signature)

(Co-Advisor)

¹ Declaration of Ethical Conduct in Research: I, as a graduate student of DGIST, hereby declare that I have not committed any acts that may damage the credibility of my research. These include, but are not limited to: falsification, thesis written by someone else, distortion of research findings or plagiarism. I affirm that my thesis contains honest conclusions based on my own careful research under the guidance of my thesis advisor.

Synthesis and Characterization of Type II core/shell Nanocrystals for Quantum-Dot- Sensitized Solar Cells

Soo Jin Kim

Accepted in partial fulfillment of the requirements for the degree of
Master of Science.

04.12. 2014

Head of Committee _____(Signature)

Prof. Jong-Soo Lee

Committee Member _____(Signature)

Prof. Nak Cheon Jeong

Committee Member _____(Signature)

Prof. Hochun Lee

MS/ES

김 수 진. Soojin Kim. Synthesis and Characterization of Type II core/shell Nanocrystals for Quantum-Dot-Sensitized Solar Cells.

201324003

Department of Energy Systems Engineering. 2015. 44p. Advisors Prof. Lee, Jong-soo Prof. Co-Advisors. Lee, Hochun, Jeong, Nak Cheon,

Abstract

In these work, type-II ZnSe/CdS core/shell nanocrystals (quantum dots, QDs) are explored as sensitizers for Quantum-Dot-Sensitized Solar Cells. Type-II ZnSe/CdS QDs synthesized by hot injection method offered low-cost and mono-dispersed QDs. Type-II QDs were expected to have the special electron-hole pair separation character as sensitizers in QDSSCs that are fundamentally different from the type-I QDs. Among their advantages is the broad absorption range in the solar irradiation spectrum and efficient carrier extraction. The result shows that multicomponent type-II ZnSe/CdS Core/Shell QDSSCs reach to higher J_{sc} value (3.49 mAcm^{-2}) than J_{sc} value (2.6 mAcm^{-2}) of single component CdSe QDSSCs. For the counter electrode of QDSSCs, Cu_2S nanocrystals were applied to improve the catalytic activity. I also reported characteristic of Sb_2S_3 which is promising sensitizer materials for QDSSCs. Colloidal amorphous Sb_2S_3 nanoparticles were synthesized and transition to crystal were obtained after annealing process. FeS_2 are also potential materials for photovoltaic materials. FeS_2 NCs were synthesized by hot injection method and nanoparticles were obtained with a diameter of $\sim 2 \text{ nm}$ and UV-Vis-NIR absorption of FeS_2 NCs shows a wide absorption up to 1400 nm .

Keywords : Quantum dot sensitized solar cell, type-II Core/Shell nanocrystals quantum dots, ZnSe/CdS Type-II Core/Shell, Sb_2S_3 NPs, FeS_2 NCs

Contents

Lists

Abstract	i
List of contents	ii
List of tables	iv
List of figures	v
1. Introduction	1
2. Background	3
2.1 Solar Cells	
2.2 Quantum Dots	
2.2.2 Properties of quantum dots	
2.2.3 Multicomponent Nanocrystals	
2.3. Quantum Dots-Sensitized Solar Cells	
2.3.1 Operation of the QDSSCs	
3. Experiment	14
3.1 Materials	
3.2 Synthesis of NCs	
3.2.1 Synthesis of CdSe QDs	
3.2.2 Synthesis of ZnSe QDs	
3.2.3 Overcoating with CdS	
3.2.4 Synthesis of Cu ₂ S QDs	
3.2.5 Synthesis of Sb ₂ S ₃	
3.2.6 Synthesis of FeS ₂	

3.3 Fabrication of photo electrode	
3.4 Fabrication of counter electrode	
3.5 Assembly of the QDSSCs	
3.6 Material Characterization	
4. Result and discussion	21
4.1 CdSe Quantum-Dot-Sensitized Solar Cells	
4.1.1 Optical analysis-CdSe nanocrystals	
4.1.2 Cu ₂ S Nanocrystals	
4.1.3 Photovoltaic measurement - CdSe QDSSCs	
4.2 ZnSe/Cds Type II core/shell nanocrystals	
4.2.1 Optical analysis - ZnSe NCs and ZnSe/CdSe NCs	
4.2.2 Photovoltaic measurement - ZnSe/Cds Type II core nanocrystals QDSSCs	
4.3 FeS ₂ Nanocrystals and Sb ₂ S ₃ nanoparticles for promising materials for QDSSCs	
4.3.1 FeS ₂ Nanocrystals	
4.3.2 Sb ₂ S ₃ Nanoparticles	
5. Conclusions	39
Summary	40
References	41

List of tables

Table 2.1 Properties of semiconductors and Quantum Dots

Table 4.1 Photovoltaic properties of CdSe QDSSCs measured 1 sun illumination

Table 4.2 Photovoltaic performance of ZnSe/CdS type II Core/Shell QDSSCs
measured 1 sun illumination.

List of figure

Fig 2.1 Best research solar cell efficiencies. Compiled by Lawrence L. Kazmerski, National Renewable Energy Laboratory (NREL), Golden, CO.

Fig 2.2 The structure of Dye-sensitized solar cells.

Fig 2.3 Schematic representation of the system of a type-I QD and type-II QD core/shell quantum Dots (QDs).

Fig 2.4 Schematic illustration of structure of Quantum-Dot-Sensitized Solar Cells (QDSSCs).

Fig 4.1 Schematic representation of the system consists of a type-II CdTe/CdSe.

Fig 4.2 Properties of CdSe NCs. (a)(b) TEM image of as-synthesized CdSe NCs. (b) X-ray diffraction patterns of CdSe NCs. (d)UV-Vis-NIR absorption and photoluminescence (PL) spectrum of CdSe NCs in Toluene. Excitation peaks at 555nm, and emission spectra is showed at 562nm.

Fig 4.3 Optical characterization of Cu₂S NCs. (a) UV-Vis-NIR absorption of Cu₂S NCs shows a wide absorption up to 1000nm, (b) TEM image of Cu₂S NCs with an average diameter of 4-5nm.

Fig 4.4 Photocurrent–voltage characteristics of CdSe QDSSCs with Cu₂S NCs CE, measured under AM 1.5 illumination (100 mWcm⁻²). The solution for ZnS passivation was

dissolved in water for CdSe-1 comparing methanol and ethanol dissolved solution for CdSe-2.

Fig 4.5 (a) Absorption spectrum, (b) photoluminescence spectrum of colloidal ZnSe NCs and ZnSe/CdS NCs, (c)(d) TEM image of ZnSe NCs and ZnSe/CdS NCs with an average diameter of 2nm and 6nm, respectively. The inset shows the average size distribution of ZnSe/CdS NCs based on dynamic light scattering (DLS).

Fig 4.6 (a)(b) Transmission electron micrographs and (inset) showing FFT patterns. (C) Energy dispersive X-ray (EDX) analysis at 300 kV (Cd, Cadmium; Zn, Zinc; Se, Selenium; S, Sulfur). (d) Electron diffraction patterns of ZnSe/CdS NCs.

Fig 4.7 Time-resolved transient fluorescence spectra of CdSe and ZnSe/CdS in toluene.

Fig 4.8 Photocurrent–voltage characteristics of ZnSe/CdS QDSSCs with Cu₂S NCs CE, measured under AM 1.5 illumination (100 mWcm⁻²).

Fig 4.9 Properties of FeS₂ NCs. (a) UV-Vis-NIR absorption of FeS₂ NCs shows a wide absorption up to 1400nm, (b) TEM image of FeS₂ NCs with an average diameter of 2nm.

Fig 4.10 Optical properties of Sb₂S₃. (a) TEM image of amorphous, orange, Sb₂S₃ nanoparticle with an average diameter of 20nm, (b)(c)(d) TEM image of crystalline Sb₂S₃ NCs after annealing at 200 °C, 250 °C, 300 °C for 1 hour (inset HR-TEM).

Fig 4.11 Temperature dependence XRD patterns of Sb₂S₃ films: Sb₂S₃ nanoparticles were

deposited to glass substrate and annealed at 100 °C, 150 °C, 200°C, 300°C, 350°C, separately.

The phase transition appeared from 150 °C and XRD patterns of samples annealed from 200 °C to 350 °C indicate that samples were crystallized.

1. Introduction

Recently the importance of renewable green energy development is increasing due to the fossil fuel depletion which is supplying most part of the global energy. The emission of greenhouse gases increased from the use of fossil fuels is also serious environmental pollution problems. Sustainable green technology is emerging to develop of renewable and eco-friendly energy sources. Among the green energy, solar energy is the one of the most promising energy. Solar cells are expected to solve the future energy problems since they utilize the unlimited solar light and do not produce any pollutants including the greenhouse gases. The first solar cells made of crystalline silicon solar cells were developed in the United States of Bell Labs in 1954 [1]. These silicon based solar cells are the first generation solar cells. These first generation solar cells make up around 90% of the photovoltaic (PV) market today [2]. In spite of the high conversion efficiency, many studied have developed to replace the crystalline silicon solar cells due to their expensive production cost. Thin film solar cells solar cells, which are called the second generation, utilize inorganic thin film structure in the cell assembly. They are consist of amorphous silicon solar cells, cadmium telluride (CdTe) solar cells, gallium arsenide (GaAs) solar cells, copper indium gallium selenide (CIGS) solar cells made of promising new materials. The second generation solar cells have high conversion efficiency and also low production cost. The third photovoltaics are expected to have a higher efficiency with lower production cost. The third generation solar cells include organic solar cells (OSCs), dye-sensitized solar cells (DSSCs) and

quantum dot-sensitized solar cells (QDSSCs) [1, 3, 4]. Low-cost and high-efficiency solar cells were first introduced with DSSCs and quantum dot (QD) was introduced as a replacement of dye in DSSCs due to its excellent opto-electronic properties. However, the third generation photovoltaics have many challenges due to the low conversion efficiency and low stability [5]. The physical and chemical properties of QDs are size-dependent. Among the advantages of QDs band gap tuning, narrow emission spectrum, good photostability, broad excitation spectra, high extinction coefficient and multiple exciton generation are included. With these advantages, QD related solar cells were achieving efficiency up to 7% [6].

In this work, CdSe QDSSCs and type-II ZnSe/CdS QDSSCs were fabricated and studied with Cu₂S nanocrystals counter electrode for broad absorption and efficient carrier extraction. In the case of CdSe QDSSCs, conduction band of CdSe is very similar to conduction band of TiO₂ which reach to make difficult to inject electron from QDs to wide-band gap semiconductor. While in the systems of ZnSe/CdS QDSSCs which have a type-II nanostructures, electron is mostly confined to the core, while the hole is mostly confined to the shell [7]. These type-II QDs were expected to have the special electron-hole pair separation character and obtained high short circuit current density. In this way, the absorption spectrum can be broadened without the decreasing of the electron extraction efficiency [5]. The synthesis of Sb₂S₃ and FeS₂, Cu₂S nanomaterials were experimented for photoanode materials and counter electrode materials in QDSSCs, respectively.

2. Background

2.1 Solar cell

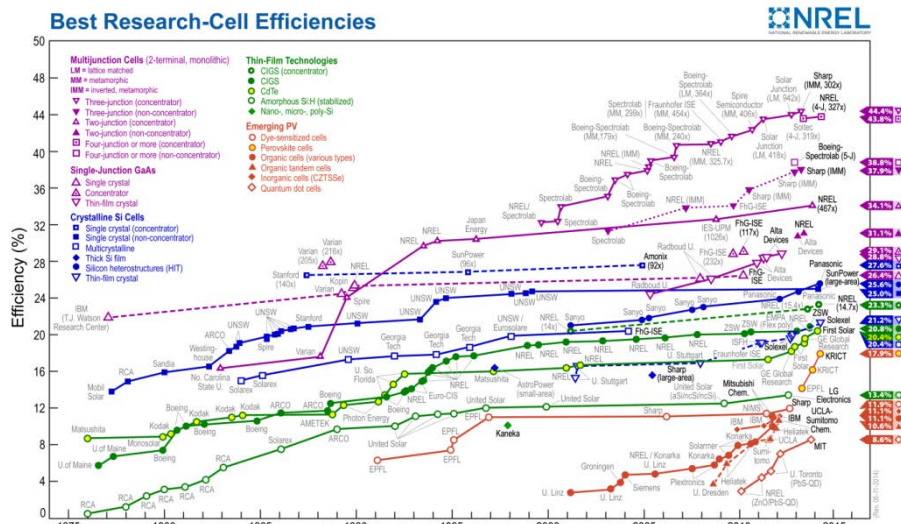


Fig 2.1 Best research solar cell efficiencies. Compiled by Lawrence L. Kazmerski, National Renewable Energy Laboratory (NREL), Golden, CO.

The graph above is from National Renewable Energy Laboratory (NREL) and shows the best research cell efficiencies with a variety type of solar cells (Fig 2.1). Although the solar market is currently dominated by different types of crystalline silicon (90%) [2], many studies exploited other materials for photovoltaics. Multi-junction solar cells are currently the recorded high efficiency with 44.4% and preferred type of solar cell for applications [8]. Except for silicon based solar cells, there are a variety of solar cells such as thin film solar cells, CdTe solar cells, organic photo voltaic cells, and DSSCs [9].

1st Generation Solar Cells

Solar cell technologies are traditionally divided into three generations. First generation solar

cells are mainly based on silicon wafers and typically have the efficiency about 15 - 20 %. These types of solar cells dominate solar panel market and are available for residential use which is seen on the rooftops. Generally, silicon based solar cell technology lie in their good performance, longer lasting than non-silicon based cells. However, they are hard to apply on flexible film and require a lot of energy in production. Generally, there are two types of first generation solar cells by dividing crystallization levels. The whole wafer of single crystal solar cells is only one crystal. If wafer consist of crystal grains, it is multi crystal solar cell.

2nd Generation Solar Cells

Thin film solar cells

The second generation solar cells are usually called thin-film solar cells. The second generation solar cells are based on amorphous silicon, CIGS and CdTe, which show the efficiency around 20%. The benefit of the second generation solar cells are low production cost because of avoiding use of silicon wafers and a lower material consumption comparing to the first generation. And the second generation solar cells can also be flexible to some degree where having many applications. However, vacuum processes and high temperature treatments lead to high energy consumption during the manufacturing processes of second generation solar cells. Further, these type of solar cells are based on scarce elements and this is a limiting factor in the price [10-12]. One of the second generation solar cells, Cadmium Telluride (CdTe), a member of the II-IV family of semiconductors, and is a promising materials for Thin-Film solar cells due to its large optical absorption coefficient,

easy to doped, and optimum band gap for solar energy conversion. Among the advantages, a CdTe film only needs 1-2 micrometers thick in order to absorb 100% of the incident solar radiation because of large optical absorption coefficient. These thin-films can then be placed on numerous types of substrates such as plastic, metal, or glass. CdTe based thin film solar cells have reached an efficiency of 16.5% as show in the figure above, which makes them alternative energy to fossil fuels. However, CdTe still has toxicity problems [13].

3rd generation solar cells

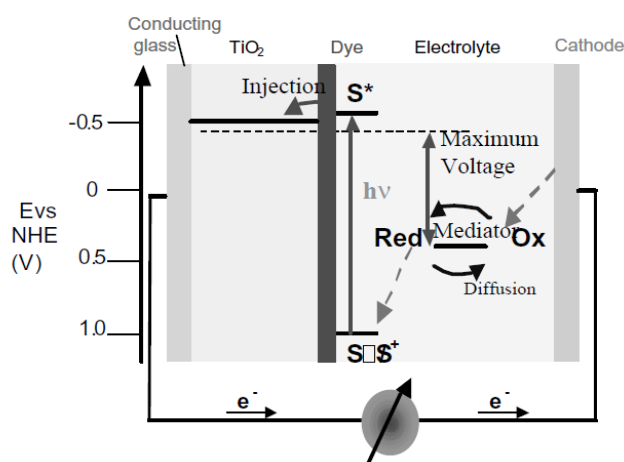


Fig 2.2 The structure of Dye-sensitized solar cells [14]

Third generation solar cells are predicted that third generation solar cells are the higher efficiency devices with lower production cost. Some examples of third generation solar cells are organic solar cells, dye-sensitized solar cells (DSSCs), quantum dot-sensitized solar cells (QDSSCs), colloidal quantum dot solar cells (CQD) etc [6]. Organic solar cells have lots

of advantages such as a simple, quick and low cost large-scale production and using of inexpensive materials. The best advantages of organic solar cells are production technologies possible to reduction price of process. The organic solar cells are fabricated through roll-to-roll (R2R) technologies comparing to the printing technology. The third generation solar cells are still needed to develop the performance and stability which is relatively lower than first and second generation solar cells. However, they have huge potential for future solar cells. One of the third generation solar cells are the Dye-sensitized solar cells (DSCs). The dye-sensitized solar cells were invented by Michael Grätzel, together with Brian O'Regani in 1991 at EPFL, Switzerland. They demonstrated that a low cost solar cell fabricated by the photo sensitization of wide band gap semi-conductors. These cells have a type of photo-electrochemical system [15]. The semi-conductor photo-sensitized is in contact with a solution containing an ionic redox couple, the I_3^- / I^- (iodide/tri-iodide) couple. DSCs record the efficiency up to 12% for small cells and about 9% for mini modules. DSCs offer the possibilities to fabricate the solar cells with a large flexibility in different shape, color, and transparency. DSCs are expected to alternative the p-n junction photovoltaic devices technically and economically with advantages [2].

2.2. Quantum Dots

Quantum dots are colloidal semiconducting nanostructure materials with diameters in the range of 2-10nm nanometers corresponding to 10 to 50 atoms. Self-assembled quantum dots are typically between 10 and 50 nm in size. They were first discovered in 1980 by Alexei Ekimov. Quantum dots confine the motion of conduction band electrons, valence

band holes, or excitons in all three spatial directions. Consequently, quantum dots show unique electronic properties, intermediate between bulk semiconductors and discrete molecules [16]. Table 2.1 shows the characteristics Quantum Dots and bulk materials.

Table 2.1 Properties of semiconductors and Quantum Dots

Properties	Semiconductor	Quantum Dot
Size	Bulk material	Nanocrystalline semiconductor, 2-10nm nanocrystalline
Electrons Energy levels	Quasi continuous	Small band gap is discrete between the valence band and conduction band
Band gap	Smaller than Quantum Dots	Tunable band gap by the composition, and size (larger band gap means bluer wavelength)
Absorbance	Uniform absorption spectrum	A series of overlapping peaks (larger at shorter wavelength)
Conversion Efficiency	31% (Shockley- Queisser)	66% (Shockley Queisser) Higher Voltage or current (Multiple exciton generation)

2.2.1 Properties of Quantum dot

Among the notable properties of quantum dots are quantum-dot confinement effect. Quantum confinement is the set of condition when the size of the radius of the semiconductor nanocrystal is less than the exciton Bohr radius. The quantum confinement of electrons and holes leads to size-dependent electronic energy levels, which treated as discrete atomic-like energy states. The size-dependence of electronic energy levels means that the size of the quantum dots decreases, the band gap of quantum dots increases. This effect offers the flexibility to control the optical, electrical properties of semiconductor

quantum dots by changing their size, and hence, manipulating their effective band gap energy. The band gap energy of the quantum dots widens with decreasing their size resulting in a color shift from red to blue. Therefore, quantum dots have attracted widespread attention due to their outstanding opto-electronic properties. The position of the lowest energy absorption spectrum can be tailored by changing their size, corresponding to the lowest energy electronic transition in the quantum dots, shifts towards higher energy. With these remarkable advantages, quantum dots are attractive for photovoltaic applications [16, 17].

2.2.2 Multicomponent nanocrystals

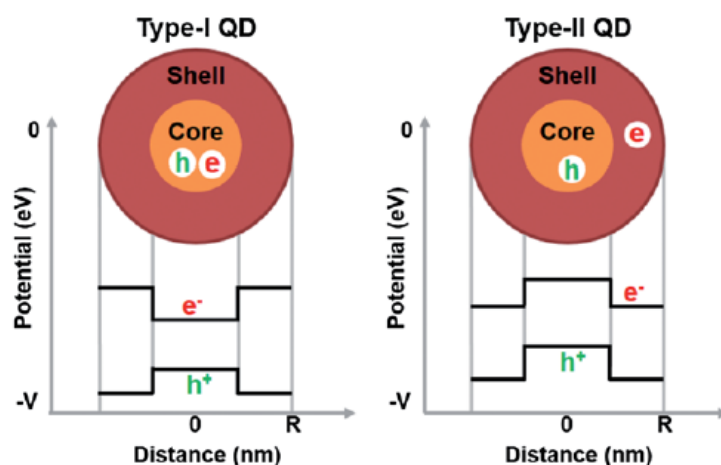


Fig 2.3 Schematic representation of the system of a type-I QD and type-II QD core/shell quantum Dots(QDs) [18].

Combining two or more semiconductor materials in a single heterojunction colloidal quantum dots such as CdTe/CdS, CdTe/CdSe QDs enhances the design of nanocrystals with

adjustable electronic and optical properties. Based on this strategy, various heterostructure nanocrystals, such as core/shell type-I and type-II quantum dots nanocrystals have been synthesized and exploited for many applications. If the shell possesses a higher band gap than the core material and the band offsets of the core/shell structures are type-I. As a result, both electrons and holes are confined in the cores [19]. A type-II QD, in contrast, has both the valence and conduction bands in the core lower (or higher) than in the shell. As a result, one carrier is mostly confined to the core, while the other is mostly confined to the shell. In recent years, novel core/shell type-II quantum dots have attracted considerable interest for their special electron–hole pair separation character, which is expected to enhance the electron extraction efficiency. The creations of a type-II core/shell quantum dots greatly enhance charge separation and increase the exciton concentration, lifetime of hot electrons, and therefore, these structures are attractive for applications of nanocrystals in photovoltaic technologies and expected to improve the performance of sensitized solar cells. Recent demonstrations of type-II colloidal core/shell nanocrystals include such as CdTe/CdSe, CdTe/CdS, CdTe/CdSe, ZnTe/CdS, and ZnTe/CdTe which have shown that greatly enhanced charge separation [5, 7].

2.3 Quantum Dots-Sensitized Solar Cells

Numerous designs for QD-based solar cells were proposed including photoelectrochemical cells such as Quantum-Dot-Sensitized Solar Cells (QDSSCs). The major advantage of QDSSCs is size-dependent absorption spectrum. QDSSCs also offer low-cost methods

synthesized mono-disperse inorganic nanocrystal sensitizers. Quantum dots are expected to enhance the cell stability comparing traditional molecular dyes in dye-sensitized solar cells (DSCs) [5]. Quantum dots act as photosensitizers and charge transport materials for QDSSCs and have a lot of advantages. First, the electronic states of the quantum dots can design to enhance spectrum between their absorption and solar spectrum. Second, fast electron and hole transfer at interfaces can be expected because of the large intrinsic dipole moments of the quantum dots. Among the advantage of quantum dots, there is a multiple electron–hole pairs (exciton) generation (MEG) [20]. QDSSCs have attracted due to the three advantages described above and as well as with their low production cost, and easy processing. Short-band-gap semiconductor QDs can harvest visible light energy assembled onto metal-oxide surfaces. CdS, CdSe, PbS, and InP semiconducting quantum dots (QDs) have preferred as photosensitizers for QDSSCs. Cadmium chalcogenide (CdX, X=S, Se or Te) QDs are attracting interest for QDSSCs research. Because CdX QDs have remarkable properties such as ease of fabrication, possible multiple exciton generation and optical and electrical properties can be easily controlled through quantum confinement effects by means of size. It is demonstrated that CdX absorbs photon efficiently due to their bulk material band gap above 1.3 eV (band gap for CdS, CdSe and CdTe are 2.25 eV, 1.73 eV and 1.49 eV respectively). In the case of QDs, a desired band gap range can be tuned by changing their size [21-23]. However, despite many advantages, QDSSCs show low energy conversion efficiencies due to the possible fast recombination through the defect states existing in the

QDs limiting electron harvesting. Therefore, many researches should be conducted to develop the efficient electrode materials, QDs, for the commercialization of the QDSSCs.

2.3.1 Structure of the QDSSCs

(1) Transparent conducting oxide

Transparent conducting oxide influences the efficiency of QDSSCs with transparent substrate and its resistivity. It is widely applied to QDSSCs due to their high conductivity and high transparenence in visible region. Transparent and conductive oxides (TCO) used in QDSSCs mainly divided two different type: indium-doped tin oxide (ITO) and fluorine-doped tin oxide (FTO). Although, early researches have been studied QDSSC performance with influence of these materials, the choice of an appropriate TCO still needs many investigations due to the large range of cell configurations and materials utilized [24].

(2) Wide-Band gap Nanostructures

For the photoanode of QDSSCs, nanostructure of mesoporous films, nanorods, nanowires and nanotubes are most commonly used for providing a large microscopic surface area. Mesoporous TiO_2 films most commonly are used for QDSSCs and prepared from paste by screen printing and the doctor blade method of solution by electrophoretic deposition. Mesoporous TiO_2 films consist typically of crystals with a diameter of 10-20nm which are sintered or pressed to form the anatase phase. The open circuit voltage is determined by the difference between Fermi level of wide-band gap semiconductor and the Fermi level of redox couple. Therefore, the higher conduction band (CB) of wide-band gap semiconductor is preferred to obtain a higher open circuit voltage. In addition, the conduction band of

semiconductor material is lower than the LUMO level of quantum dots materials for easier transfer. TiO_2 , SnO_2 , ZnO , Nb_2O_5 have been exploited for used of wide-band gap semiconductor [17].

(3) Electrolyte

The most commonly used electrolytes in QDSCs are aqueous polysulfide [20]. Besides, the $\text{Fe}^{3+}/\text{Fe}^{2+}$ and the $\text{Fe}(\text{CN})_6^{3-}/\text{Fe}(\text{CN})_6^{4-}$ redox systems, both in aqueous solution, have been exploited in conjunction with CdS-sensitized cells. Solid-state hole conductors such as spiro-OMeDAT and CuSCN have been studied to replace the liquid electrolyte.

(4) Counter electrode

Platinized TCO layers have been utilized in conjunction with all of the redox electrolytes in QDSSCs mentioned above. For the polysulfide electrolyte the Pt counter electrode leads to a rather low fill factor and Au has been used alternatively. Hodes et al. investigated metal sulfides (especially Co, Cu and Pb) as suitable counter-electrode materials, measured their long-term stability.

2.3.2 The operation of QDSSCs

QDSSCs performance is decided by Interfacial Charge-Transfer Processes. One of the key factors to determine QDSSCs performance is efficient electrons and holes transport to the electrodes. The fast electrons transfer to oxide layer and holes to hole transport layer or redox couple are the important factor for the photon conversion efficiency. The overall power conversion efficiency are determined by loss of electrons through interfacial recombination processes and discharge of electrons at the counter electrode. Figure 2.4 shows operation

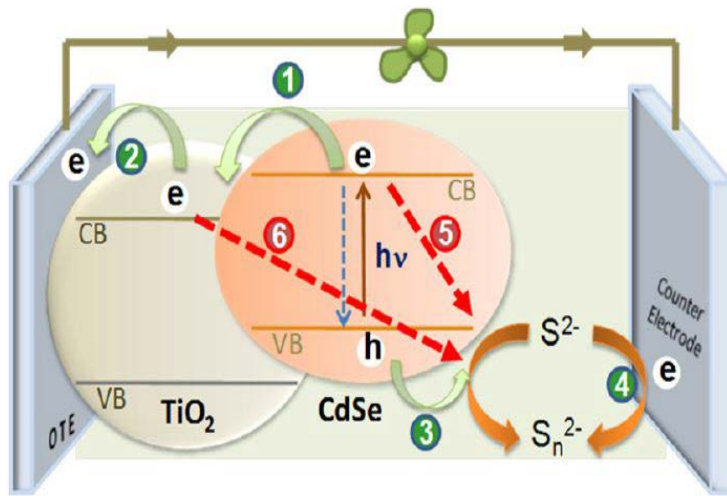


Fig 2.4 Schematic illustration of structure of Quantum-Dot-Sensitized Solar Cells(QDSSCs) [25]

steps of a CdSe QDSSCs that determine the overall efficiency applying S^{2-}/Sn^{2-} redox couple. These include (1) QDs attached to the surface of a mesoporous TiO_2 (wide-bandgap semiconductor) absorbs light and then excited electrons injects into the conduction band of metal oxide nanoparticle, TiO_2 . (2) The electrons transport through its nanoparticle network by diffusion to the current collector (anode), and then pass through the external circuit,(3) next step is hole transfer to redox couple in the electrolyte and (4) regeneration of the redox couple at the counter electrode.

3. Experiments

3.1 Materials

All chemicals used in the experiments were of the highest purity grade available and were purchased from Sigma-Aldrich.: selenium(powder, 99.99%, Aldrich), cadmium oxide (CdO, 99% Aldrich), diethyl Zinc(1.0M in hexanes), trioctylphosphine (TOP, 97%, Strem), oleic acid (OA, 90%, Aldrich), trioctylphosphine oxide (TOPO, 99%, Aldrich), 1-octadecene (ODE, 90%, Aldrich), oleylamine (97%, Aldrich), dodecanethiol (98%, Aldrich), copper(II) acetylacetonate(99.99%, Aldrich), ammonium diethyldithiocarbamate(Aldrich), antimony(III) chloride(SbCl_3 , 99.99%, Aldrich), sulfur (99.998%, Aldrich), octylamine(99%, Aldrich), Iron(III) chloride(FeCl_3 , 97%, Aldrich), 1,2-Hexadecanediol, (technical grade, 90%, Aldrich)

3.2 Synthesis of NCs

3.2.1. Synthesis of CdSe QDs

Colloidal CdSe NCs were synthesized via hot injection method. A selenium solution was prepared by elemental Se (0.7896 g) with an excess amount of TOP (10 mL), and then solution was stirred in a glove-box at room temperature to generate a clear 1 M solution of TOP-Se. For the synthesis of the cadmium oleate complexes, the mixture of cadmium oxide and oleic acid was degassed at 100 °C and then heated to 220 °C to dissolve the cadmium oxide under nitrogen gas. For the synthesis of CdSe QDs, 3ml of 0.5M Cd(oleate)₂, 2.2g of TOPO was added to the 16ml ODE in a three-neck flask, and the mixture was heated to

100 °C for 1 hour with vigorous stirring under vacuum to dissolve the mixture perfectly. After a change in the nitrogen atmosphere, the temperature was raised to 300 °C. The 6 ml of oleylamine was injected into the reaction three-neck flask at 300 °C. The 8 ml TOP-Se solution (1.0 mmol in TOP) was injected quickly into the mixed solution at 300 °C and the reaction flask was held at this temperature for 3 min. After the reaction mixture was allowed to cool to 50 °C, the subsequent cleaning of nanocrystals was performed by hexane/ethanol extraction to remove unreacted precursor and undesirable synthesis. 10 ml-20 ml of ethanol was slowly added to the reaction mixture in hexane, which was then centrifuged for 5 min at 4500 rpm. This washing was repeated three times, the NCs were re-dissolved in toluene [21].

3.2.2 Synthesis of ZnSe QDs

The oleylamine (7 ml) was heated to 120 °C for 1 hour in three-neck flask with vigorous stirring under vacuum to synthesis of ZnSe NCs. The solution was heated up to 325 °C under nitrogen flow, followed by a quick injection of a mixed solution with 0.5 ml TOP-Se and 0.5 ml Zn(Et)₂. The reaction was held at 300 °C for 10 min. After the reaction mixture was allowed to cool to 50 °C, the ZnSe nanocrystals were precipitated by Toluene/Acetone with three times to remove unreacted precursor and undesirable synthesis. The final solutions were re-dispersed in the toluene.

3.2.3. Overcoating with CdS

The CdS shell was grown using a layer-by-layer growth technique in a one-pot synthesis. For shell deposition, injection stock solutions were prepared at a concentration of 0.1 M in 1-octadecene (ODE) and oleic acid. Cadmium was obtained by dissolving 0.3201 g of

cadmium oxide in 6.18g of oleic acid and 18ml of ODE in a three-neck flask under vacuum by heating it to 100 °C for 1hr. The solution was heated up to 230°C while stirring. After the solution became clear, it was cooled to 60 °C. The sulfur injection solution was prepared from 0.65 g of sulfur dissolved in 20mL of ODE by heating the mixture to 100 °C under vacuum. While the ZnSe mixture is vigorously stirred under vacuum at 70 °C in the 5ml of ODE and 1ml of oleylamine, the previously prepared Cd oleate and Sulfur overcoating stock solution is added dropwise at 70°C under nitrogen atmosphere. Following the injection, the solution was heated to 225°C for 10-20 min. The ZnSe/CdS nanocrystals were washed by toluene/acetone with three times to remove unreacted precursor and undesirable synthesis. The final solutions were re-dispersed in the toluene.

3.2.4 Synthesis of Cu₂S QDs

Cu₂S NCs was synthesized with 1.25 mmol of ammonium diethyldithiocarbamate added to 10 ml of dodecanethiol and 17 ml of oleic acid (OA) in a 3-neck flask. The mixture was degassed under vacuum for 30min at room temperature and then heated up to 110 °C under nitrogen flow for 1 hour. A suspension mixture of 1 mmol of copper(II) acetylacetonate in 3 ml of oleic acid was quickly injected to the 3-neck flask. Then solution was quickly heated to 180 °C and reaction was kept at this temperature for 20min. After the reaction mixture was allowed to cool to 50 °C, Cu₂S NCs was purified by hexane/ethanol with three times and re-dispersed in anhydrous hexane kept in the glove box to avoid any possible oxidation of NCs.

3.2.5 Synthesis of Sb₂S₃

Hot injection method was used to synthesis of Synthesis of Sb₂S₃ nanoparticles. 0.228g of

SbCl_3 was mixed with 20ml of 1-octadecene(ODE) and 2ml of Oleic acid and degassed for 1 hour at 110°C in a three-neck flask. In a separate pot, an injection solution consisting of 0.16g of sulfur in 4.5ml of oleylamine and 0.5ml of octylamine was degassed at room temperature for 1 hour with vigorous stirring. The temperature of the reaction solution was then raised to 180 °C under nitrogen atmosphere. 2ml of the injection solution was added by syringe and the reaction mixture kept at 180 °C for 10 min. The reaction was then quenched with a water bath. The nanoparticles were extracted from the reaction mixture by precipitation using hexane/ethanol, which was then centrifuged for 5min at 4500 rpm with two cycles. The final nanoparticles were re-dispersed in the toluene. The solution of an amorphous, orange Sb_2S_3 was deposited onto the glass and dried at room temperature. Then, Sb_2S_3 film was heated from 100 °C to 400 °C on the hot plate under nitrogen atmosphere for 1hour. The samples of the dark brown crystalline Sb_2S_3 was formed after the annealing process.

3.2.6 Synthesis of FeS_2

For the synthesis of the FeS_2 , the mixture of 0.63g of FeCl_3 , 0.129g of 1,2-Hexadecanediol, 10ml of 1-octadecene(ODE) and 2ml of oleic acid was degassed at room temperature for 30min and then heated to 110°C to dissolve the FeCl_3 under nitrogen atmosphere. Sulfur precursor was prepared with 0.192g of sulfur in 5ml of oleylamine. 5ml of sulfur precursor was injected quickly into the mixed solution at 180 °C and the reaction flask was held at this temperature for 90min. The final solution was washed Chloroform/ethanol and re-dispersed in toluene. The solution of an amorphous, orange Sb_2S_3 were deposited onto the glass and

dried at room temperature and then heated at 100 °C to 400 °C under nitrogen atmosphere for 1 hour. The dark brown crystalline Sb_2S_3 films were formed after the annealing process.

3.3 Fabrication of photo electrode

TiCl_4 (0.09 M in HCl, Aldrich), TiO_2 paste (Ti-Nanoxide T/SP) were used for TiO_2 wide bandgap semiconductor and the sealing foil (Meltonix 1170-25) were purchased from Solaronix. Fluorine-doped tin oxide (FTO, $13\Omega \text{ sq}^{-2}$, Hartford Glass Co. Inc) glass was used as transparent conducting oxide substrate for the photo electrode and counter electrode substrate. FTO substrates were sonicated for 10min with detergent solution, washed with deionized water and again sonicated in acetone, methanol and iso-propanol for 10 min. The cleaned FTO substrates were immersed in 45 mM aqueous TiCl_4 solution in 10% HCl at 70 °C for 30 min to deposit a thin TiO_2 layer onto the FTO substrate and washed with water and ethanol. Mesoscopic TiO_2 films was prepared on FTO glass substrate by using a doctor blading TiO_2 paste on to Scotch tape with a 0.09 cm^2 hole in it, which was used as a mask and spacer. Treated substrates were dried at 85 °C, followed by calcination at 450 °C for 30 min to deposit anatase layer. Cysteine solution was prepared to attach the linker molecules to the TiO_2 surface. For cysteine a saturated solution in water was employed. Hydrochloric acid was added to increase solubility of cysteine in water [26]. After sintering, the FTO/ TiO_2 electrodes were immersed into 0.3M Cysteine Solutions containing the linker molecules for 8hr, rinsed with same solvent. For the QD sensitization, the films (TiO_2/FTO) were immersed into a CdSe NCs (4 mg/ ml) or ZnSe-CdSe NCs in toluene for 16 hour and rinsed in

anhydrous hexane. (Finally, a passivation layer of ZnS was implemented to QDs/TiO₂/FTO substrate. A layer of ZnS was applied to prevent the charge recombination from TiO₂ to electrolyte by the following chemical bath deposition. The TiO₂ electrode was dipped into a DI water solution of ZnAc₂(0.03M) for 1min, washed with DI water thoroughly to remove the excess precursor, dipped again into a DI water solution of Na₂S (0.03 M) for 1min, and washed again with DI water for 30sec. The above cycle, named successive ionic layer adsorption and reaction (SILAR), was repeated two times. ZnS passivation layer can results in the suppression of the surface trapping of photoexcited electrons and holes in the QDs. Thus, the photoexcited electrons can efficiently inject into the TiO₂ conduction band, and a higher short circuit current (J_{sc}) and IPCE values is obtained [27, 28].

3.4 Fabrication of counter electrode

The counter electrode was prepared with Cu₂S NCs. Final product of Cu₂S was re-dispersed in hexane–octane (9:1 vol) mixture solution. Cu₂S NC films were formed via drop casting onto the FTO substrate, followed by sintered at 110 °C for 1hour to evaporate the organic solvent. All processes were treated under nitrogen atmosphere.

3.5 Assembly of the QDSSCs

The photo electrode and counter electrode were assembled using a sealant (SX 1170-60, Solaronix) at 100 °C. The polysulfide electrolyte was consisted of a Na₂S (2 M) and S (2 M) dissolved in deionized water. The liquid electrolyte was injected into the cell for the Photoelectrochemical Characterization.

3.6 Material Characterization

All UV-vis absorption and photo-luminescent spectra were obtained in a quartz cuvette. The absorption spectra of the nanocrystals were obtained by a Agilent Cary-5000 UV-vis-NIR spectrophotometer. The samples were measured by diluted nanocrystals with solution solvent in Quartz cuvettes to analyze the concentration of nanocrystals. Photoluminescence (PL) was measured using a FluoroMax-4 spectrofluorometer (HORIBA Jobin Yvon). Nanocrystals were characterized by transmission electron microscopy (TEM), Hitachi HF-3300 operating at an acceleration voltage of 300 keV. The atomic arrangement was directly observed and structure was analyzed by TEM. A TEM specimen was prepared by drying each QDs solution on a lacey carbon Cu (300 mesh) grid. XRD diffraction pattern were measured by Empyrean HR-XRD with Cu K α radiation source. Samples for XRD analysis were prepared by drop casting nanocrystal solutions onto glass substrates, and detector angle was scanned onto the glass from 10 ° to 70 °. Photocurrent density–voltage (J–V) characteristics of the QDSSCs were measured using a Mcscience Inc under 1 Sun illumination (AM 1.5) with a power of 100mW/cm² verified by an AIST-calibrated Si-solar cell.

4. Results and Discussion

4.1 CdSe Quantum-Dot-Sensitized Solar Cells

4.1.1 Optical analysis - CdSe Nanocrystals

CdSe nanocrystals are well known photo-excited semiconductors quantum dots expected to have harvest light energy in the entire visible region with its tunable band edge. (The band gap of bulk CdSe is 1.65eV.) Early studies have demonstrated that maximum power-conversion efficiency was observed with 3nm diameter quantum dots because 3nm CdSe have greater charge injection rates, higher IPCE, better absorption in the visible region and also effective electron injection into TiO₂ [21]. Figure 4.2(a) shows the absorption and emission spectra of CdSe, which exhibits a lowest energy peak at 555nm and excited at 562nm. The absorption onsets showed a gradual red-shift with increasing the reaction time in the figure 4.2(a). The shifted absorbance spectra to higher wavelength suggest that CdSe quantum dots grow larger by aggregating with increasing the reaction time. The size of CdSe nanocrystals were controlled to 3nm with reaction time which was optimized 5min. Figure 4.2(b) shows a TEM image of mono-dispersed CdSe NCs with an average diameter of the 3nm.

4.1.2 Cu₂S Nanocrystals

The optical property of Cu₂S NCs shows in Figure 4.3(a). The Absorption spectra of the Cu₂S NCs shows a wide absorption up to approximately 1000 nm. Figure 4.3(b) show TEM image of monodispersed Cu₂S NCs with an average diameter of 3.5nm. For the counter electrode of QDSSCs, carbon electrode showed much higher catalytic activity beyond Pt in

polysulfide redox system (S^{2-}/S_x^{2-}) and the cell efficiency. There are other materials which have obtained better performance. Cu_2S is one of the promising counter electrode materials. In general, brass slide are used for the Cu_2S counter electrode in QDSSCs for the high fill factor (FF) and improving photovoltaic efficiency. In this study, Cu_2S nanocrystals were synthesized and applied for counter electrode for QDSSCs. The Cu_2S NCs were dispersed onto the FTO via drop casting to fabricate the Cu_2S film. The self-assembled method is used to obtain higher surface coverage. Cu_2S nanocrystals were expected to provide higher surface areas which improve the catalytic activity in the interface between polysulfide electrolytes of counter electrodes.

4.1.3 Photovoltaic measurement - CdSe QDSSCs

The current density-voltage curves show the power conversion efficiency, as different method of making photoanode under regenerative polysulfide (2 M Na_2S / 2 M S) redox couple. All the photovoltaic measurements were obtained under AM 1.5 illumination (100 $mWcm^{-2}$). The performance of the CdSe QDSSCs was measured. Table 4.1 and Figure 4.4 present the photovoltaic parameters and the current density–voltage (J–V) curves of the CdSe QDSSCs using Cu_2S nanocrystals as the counter electrode including open circuit voltage (V_{oc}), short circuit current density (J_{sc}), fill factor (FF), and the total cell efficiency (η), respectively. The cell's area was $0.09 cm^2$. The open circuit photovoltage (V_{oc}), short circuit photocurrent (J_{sc}), and fill factor (FF) of CdSe-1 QDSSCs are 0.318 V, 1.93 $mAc m^{-2}$, and 48.25, respectively, and the overall conversion efficiency is 0.29%. The bifunctional linker molecules are used to attach colloidal QDs to the TiO_2 surfaces:

mercaptopropionic acid (MPA), thioglycolic acid (TGA), and cysteine. The role of bifunctional group reduces electron tunneling injection by separation between QDs and semiconductor. Molecular structures of MPA, TGA, cysteine have thiol group(SH) and another carboxylate group(COOH), that links to the TiO₂. In this study, cysteine linker was applied to fix the colloidal QD to the TiO₂ and these linkers were expected to improve the cell performance. Cysteine has three functional groups (thiol, amino, and carboxyl), which can easily link with molecules and surfaces and high charge density on a small area [28]. In the table 4.1, the open circuit voltage (V_{oc}) with 0.318 V. The low short circuit current is most probably due to the ineffective excited-electron injection from CdSe QDs to conduction band of TiO₂ in working condition. In the case of CdSe QDSSCs, conduction band of CdSe is very similar to conduction band of TiO₂ which reach to make difficult to inject electron from QDs to wide-bandgap semiconductor. Other types of QDs were used for sensitizer to get higher short circuit current such as type II core/shell nanocrystals.

For the ZnS passivation layer, ZnAc₂(0.03M) and Na₂S(0.03M) were dissolve in methanol and ethanol respectively. And also dissolving in D.I water solution was used to passivate photoanode. Figure 4.10 shows the photo current–voltage curves of the CdSe QDSSCs for different use of ZnS passivation solution solvent. The photovoltaic parameters of the cells are shown in Table 4.1. The V_{oc} of both tested cells is almost identical. Conversely, J_{sc} was higher for D.I water solution. This suggests that solubility of ZnAc₂ and Na₂S was better in D.I water which may cause the high effect of ZnS passivation layer and may reduce electron recombination at the interface between the TiO₂ electrodes and electrolyte.

4.2 Optical analysis - ZnSe/Cds Type II core/shell nanocrystals QDSSCs

4.2.1 ZnSe NCs and ZnSe/CdSe NCs

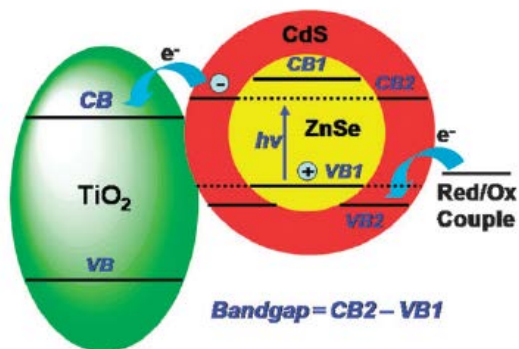


Fig 4. 1 Schematic representation of the system consists of a type-II ZnSe/CdS NCs [5]

The absorption and fluorescence spectra of the ZnSe/CdS QDs in toluene are shown in Fig. 4.5(a)(b). Absorption spectra of ZnSe and ZnSe/CdS NCs in solution were 375nm and 526nm. Fluorescence spectra of ZnSe and ZnSe/CdS NCs in solution were 387nm 542nm. It is seen that with the increase of the shell thickness, the absorption and fluorescence spectra were showed bathochromic shift. In type-I QDs like CdSe/ZnS, the photoexcited electron-hole pair are confined in the one semiconductor which shows the lowest energy states for both electrons and holes. A type-II QD like ZnSe/CdS, in contrast, carrier is mostly confined to the core, while the hole is mostly confined to the shell. Type-II QDs were expected to have the special electron-hole pair separation character as sensitizers in QDSSCs that are fundamentally different from the type-I QDs. The energy bandgap of ZnSe/CdS was determined by the CB edge of CdS and the VB edge of ZnSe (Figure 4.1). Therefore, ZnSe/CdS core/shell QDs can show better absorption spectra than either the ZnSe or CdS nanocrystals. TEM image of monodispersed ZnSe and ZnSe/CdS NCs are showed in Figure

4.5. Average diameter of ZnSe NCs and ZnSe-CdS NCs are 2nm and 6nm respectively. Therefore, shell thickness of ZnS/CdS Core/Shell was supposed approximately 2nm. The schematic representation of ZnSe/CdS Core/Shell was showed upside of the PL spectrum. The as-synthesized ZnSe/CdS NCs were nearly spherical(average diameter 6nm), which is consistent with the results obtained from DLS measurement, with size deviation below 10%(inset of Fig 4.5 right side). A representative HRTEM image of ZnSe/CdS core/shell QDs was shown in Figure 4.6(a)(b). The FFT pattern shown in the top inset of Figure 4.6(a)(b) also confirms full crystallinity of the produced ZnSe/Cds core/shell QDs. Figure 4.6(c) shows EDS result of ZnSe/CdS core-shell QDs and component of Cd, Se, Zn and S. In figure 4.6(d), selected area electron diffraction (SAED) pattern of ZnSe/CdS NCs were showed and it has ring pattern which determined that large number of perfect crystals are randomly oriented. Figure 4.7 shows the time-resolved transient fluorescence decay spectra of CdSe and ZnSe/CdS NCs recorded with 379 nm diode laser excitation. The fluorescence decay lifetimes of ZnSe/CdS NCs are much longer than single component CdSe NCs. It can be explained that spatial separation of electrons and holes in ZnSe/CdS type-II QDs result in a long fluorescence decay lifetime because of delaying the radiative recombination.

4.2.2 Photovoltaic measurement - ZnSe/Cds Type II core nanocrystals QDSSCs

Type II ZnSe/CdS QDSSCs provide suitable band alignment between QDs and wide-bandgap semiconductor. Figure 4.8 shows current density–voltage (J–V) curves of the ZnSe/CdS type II core/shell QDSSCs. The open circuit voltage (V_{oc}), short circuit current density (J_{sc}), fill factor (FF), and the total cell efficiency (η) were summarized in table 4.2. The open circuit photovoltage (V_{oc}), short circuit photocurrent (J_{sc}), and fill factor (FF) of ZnSe/CdS QDSSCs are 0.175 V, 3.5 mAcm⁻², and 46.5%, respectively, and the overall conversion efficiency is 0.28%. The low open circuit voltage is most probably due to the high recombination kinetics with the electrolyte. Although overall conversion efficiency is relatively low, the short circuit current (J_{sc}) is higher than J_{sc} of CdSe QDSSCs. It can be explained that electron is mostly confined to the ZnSe-core, while the hole is mostly confined to the CdS-shell. Therefore ZnSe/CdS Type-II QDs have the spatial electron-hole pair separation character as sensitizers in QDSSCs.

4.3 FeS₂ Nanocrystals and Sb₂S₃ nanoparticles for promising materials for QDSSCs

4.3.1 FeS₂ Nanocrystals

Pyrite iron disulfide (FeS₂) is abundant in nature and nontoxic. Therefore these materials are potential photovoltaic material candidate for solar energy conversion. Colloidal pyrite nanocrystals (NCs) were synthesized for counter electrode materials for QDSSCs. Absorption spectra was widen to near infrared (NIR) wavelengths because of its large optical absorption coefficient ($>10^5$ cm⁻¹) and narrow band gap of 0.95 eV. Solution process can be

used to fabricate to FeS₂ nanocrystals counter electrode which shows the low-cost and enable the flexible devices [29]. The optical property of FeS₂ NCs shows in Figure 4.9(a). UV-Vis-NIR absorption of FeS₂ NCs shows a wide absorption up to approximately 1400nm. Figure 4.9(b) shows a TEM image of mono-dispersed FeS₂ NCs with an average diameter of 2nm.

4.3.2 Sb₂S₃ Nanoparticles

Sb₂S₃ are narrow-band gap semiconductors, which have shown as a promising sensitizer due to its suitable energy band gap of about 1.7-1.9 eV and a strong absorption spectrum. Comparing with bulk materials, Sb₂S₃ nanoparticles can enhance power conversion efficiency due to the multiple exciton generation [30]. Sb₂S₃ nanoparticles were synthesized as described the above. As-synthesized Sb₂S₃ nanoparticles were orange colloidal solution. In figure 4.10(a-d), TEM image shows that the mono-dispersed amorphous Sb₂S₃ nanoparticles were observed and crystalline Sb₂S₃ nanoparticles obtained after annealing process. The Sb₂S₃ nanoparticles were crystallized after the annealing treatment. The sample of annealing at 200 °C is not perfect crystal. Some of particles still remained amorphous and some of particles transitioned to crystalline. In the other, the sample annealed at 300 °C is perfectly crystal nanoparticles. Inset shows the HR TEM image of Sb₂S₃ samples annealed at different temperature. And also temperature dependence X-ray diffraction (XRD) patterns of the amorphous Sb₂S₃ nanoparticles are presented in figure 4.11. The film deposited at room temperature, 100 °C and 150 °C presented amorphous structure, as it can be seen in figure 4.9. The transition of amorphous Sb₂S₃ nanoparticles to crystalline

was appeared from 150 °C in temperature dependence XRD patterns. While deposited at 200 °C to 350°C has a polycrystalline orthorhombic structure. The XRD pattern showed that the crystallinity of the thin films enhances by increasing the annealing temperature. The 350 °C annealed film presents a sharpest diffraction peak comparing to lower temperature annealed films.

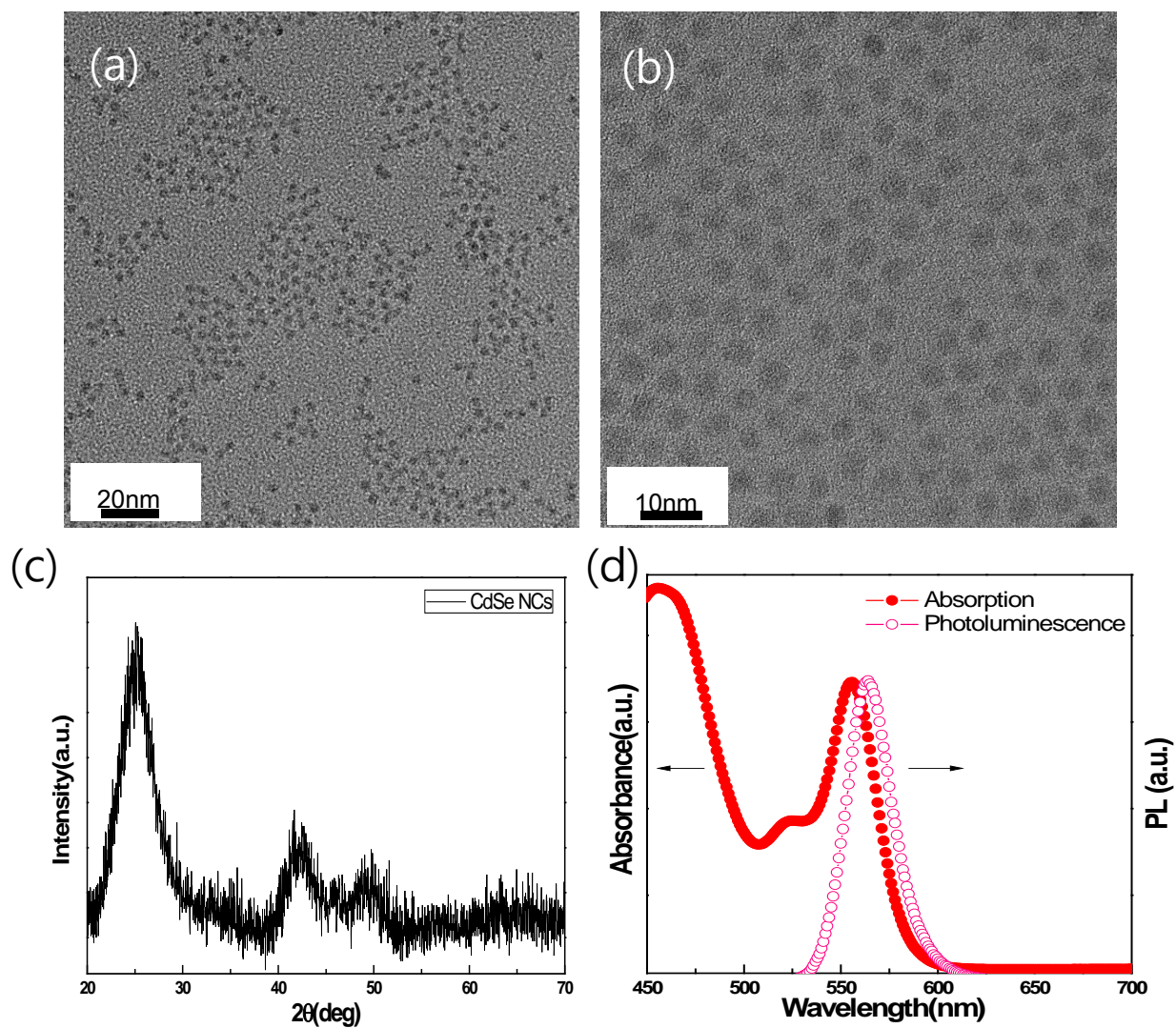


Fig 4. 2 Properties of CdSe NCs. (a)(b) TEM image of as-synthesized CdSe NCs. (b) X-ray diffraction patterns of CdSe NCs. (d)UV-Vis-NIR absorption and photoluminescence (PL) spectrum of CdSe NCs in Toluene. Excitation peaks at 555nm, and emission spectra is showed at 562nm.

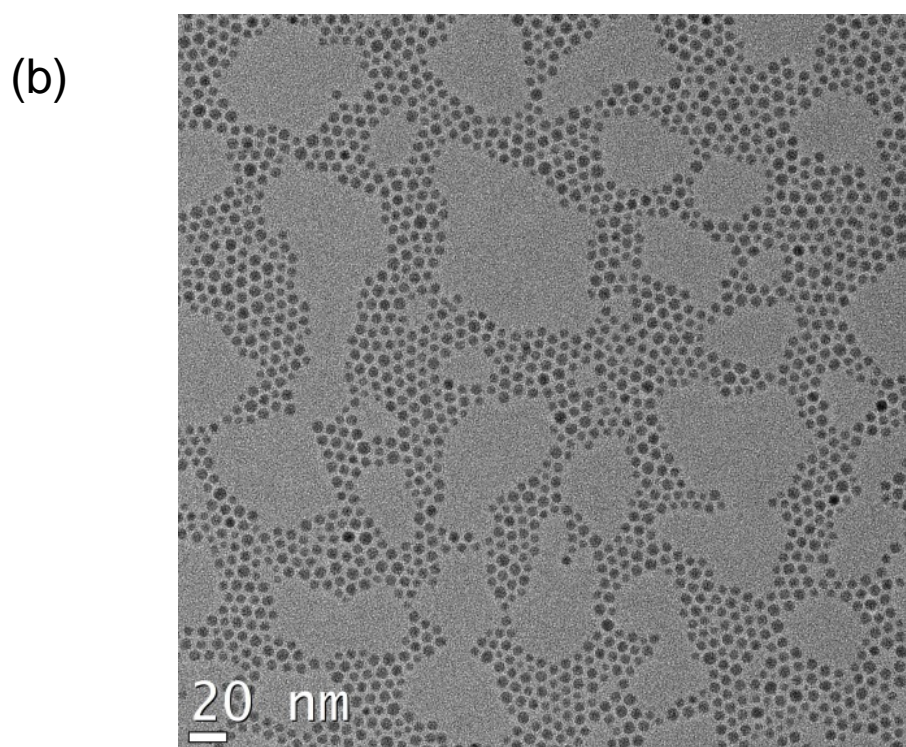
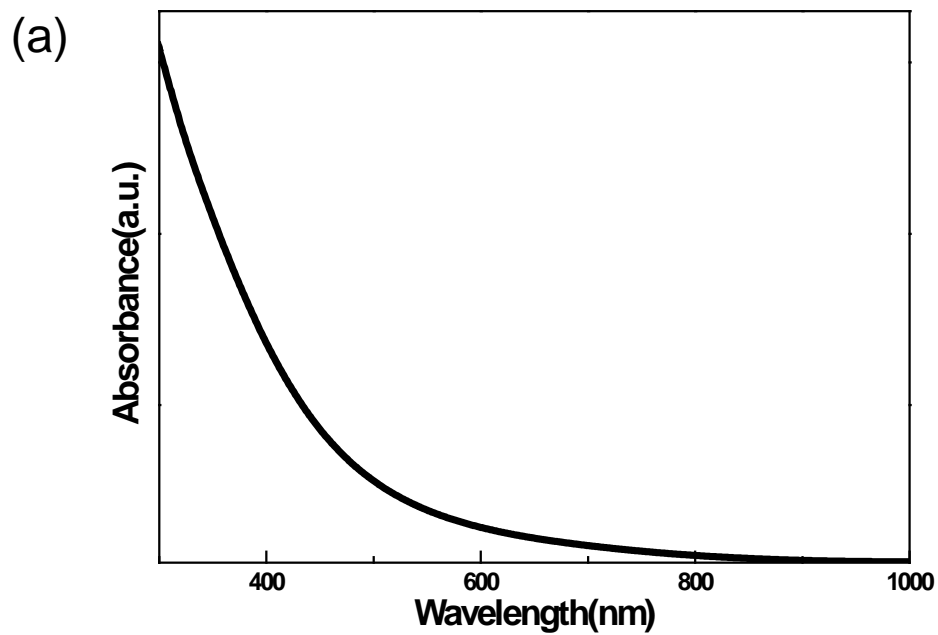


Fig 4. 3 Optical characterization of Cu₂S NCs. (a) UV-Vis-NIR absorption of Cu₂S NCs shows a wide absorption up to 1000nm, (b) TEM image of Cu₂S NCs with an average diameter of 4-5nm.

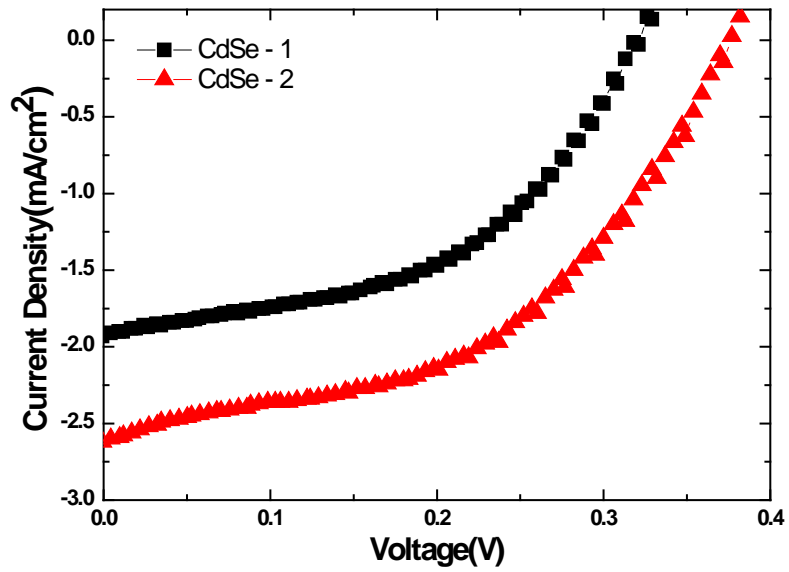


Fig 4. 4 Photocurrent–voltage characteristics of CdSe QDSSCs with Cu₂S NCs CE, measured under AM 1.5 illumination(100 mWcm⁻²). The solution for ZnS passivation was dissolved in water for CdSe-1comparing methanol and ethanol dissolved solution for CdSe-2.

Table 4. 1 Photovoltaic properties of CdSe QDSSCs measured 1 sun illumination.

Samples	J _{sc} (mAcm ⁻²)	V _{oc} (V)	FF	η(%)
CdSe-1	1.93	0.318	48.25	0.29
CdSe-2	2.6	0.377	47.158	0.465

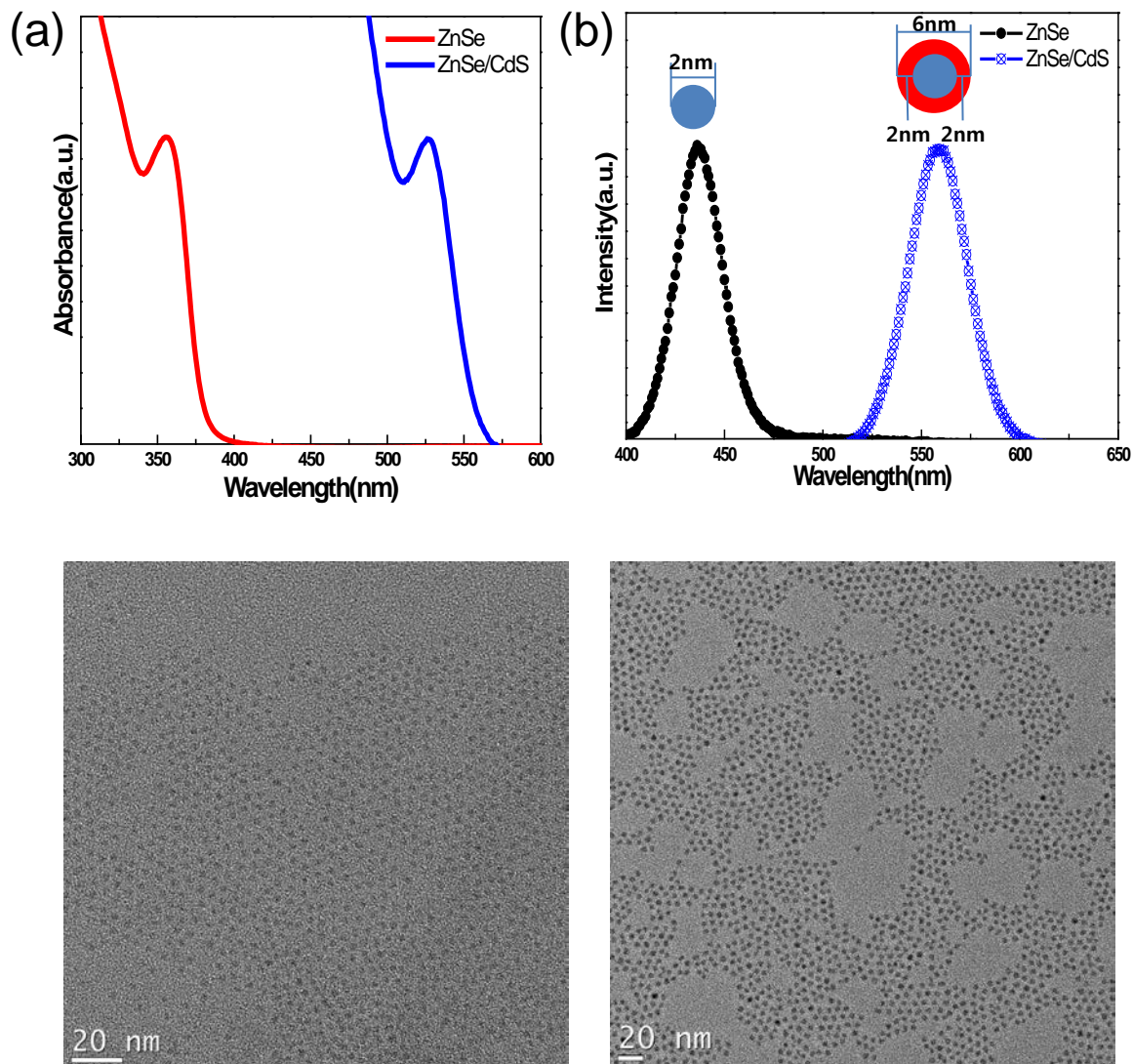


Fig 4. 5 (a)Absorption spectrum, (b)photoluminescence spectrum of colloidal ZnSe NCs and ZnSe/CdS NCs, (c)(d)TEM image of ZnSe NCs and ZnSe/CdS NCs with an average diameter of 2nm and 6nm, respectively. The inset shows the average size distribution of ZnSe/CdS NCs based on dynamic light scattering (DLS).

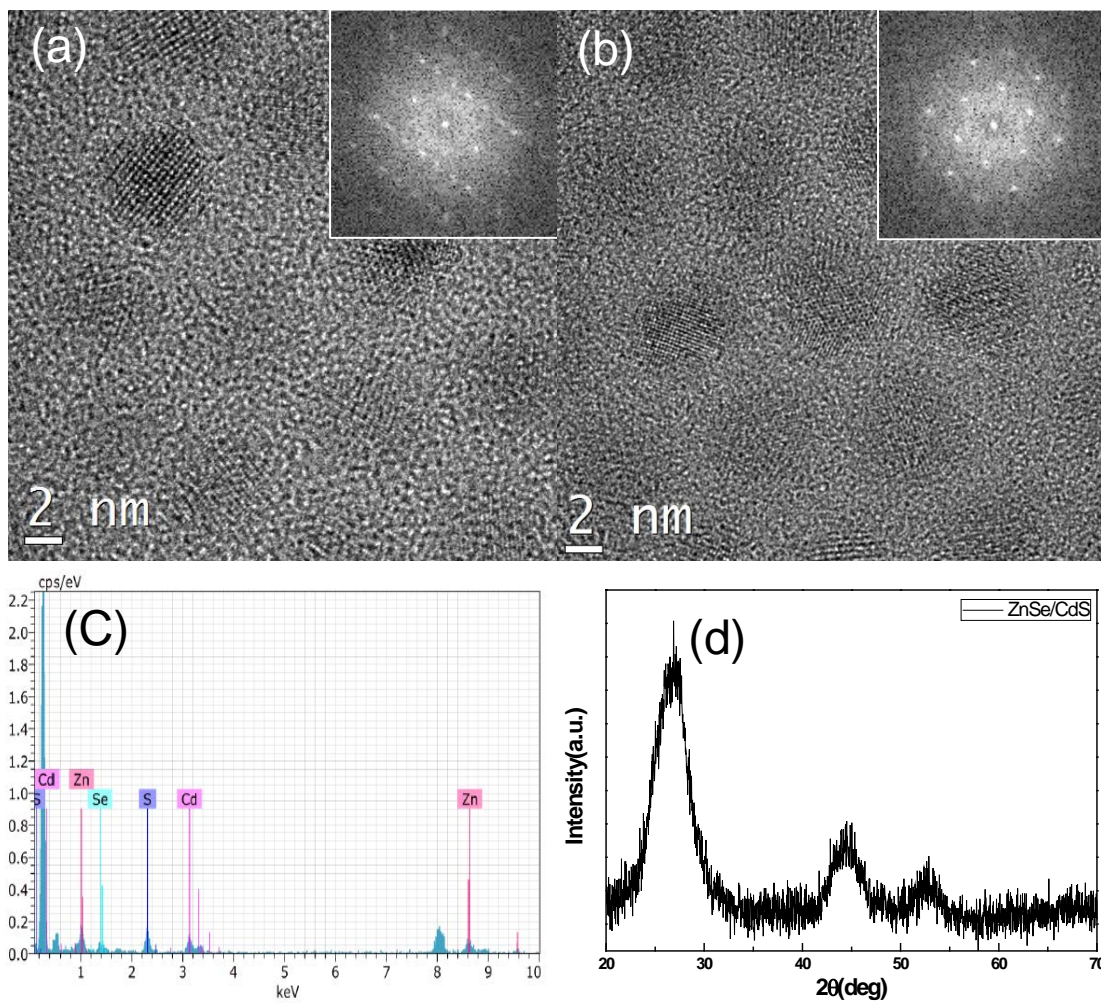


Fig 4. 6 (a)(b) Transmission electron micrographs and (inset) showing FFT patterns. (C) Energy dispersive X-ray (EDX) analysis at 300 kV (Cd, Cadmium; Zn, Zinc; Se, Selenium; S, Sulfur). (d) X-ray diffraction patterns of ZnSe/CdS NCs.

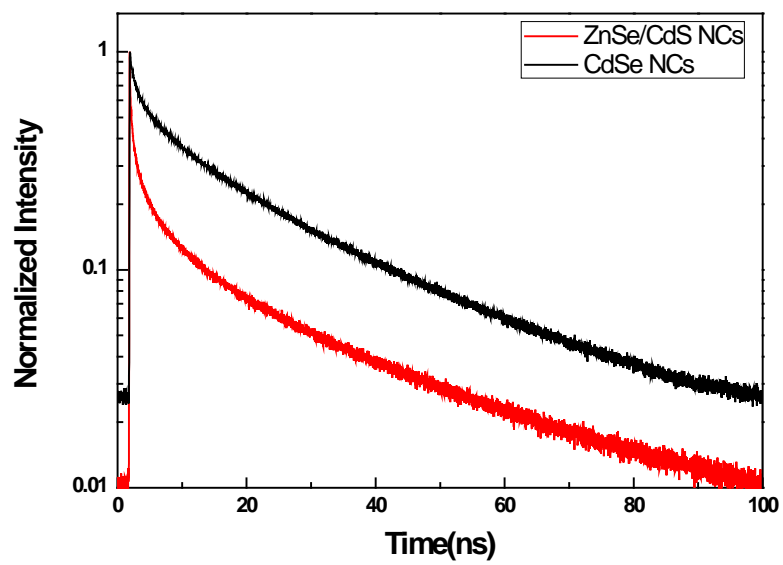


Fig 4. 7 Time-resolved transient fluorescence spectra of CdSe and ZnSe/CdS in toluene.

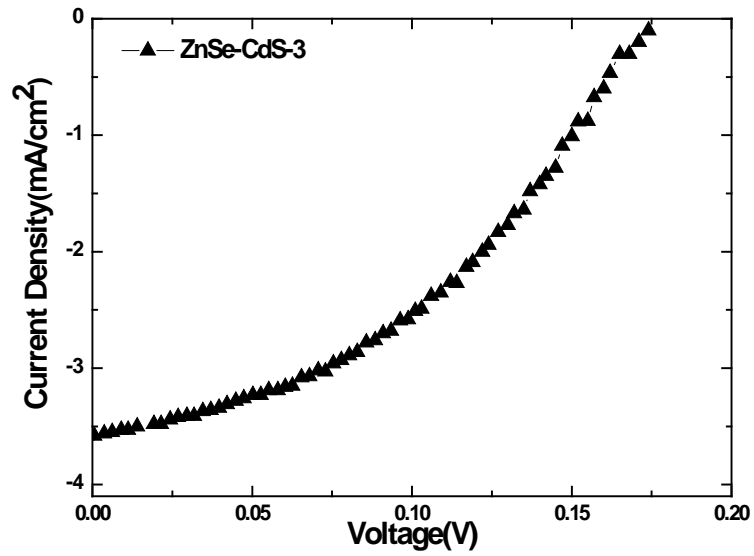


Fig 4. 8 Photocurrent–voltage characteristics of ZnSe/CdS QDSSCs with Cu₂S NCs CE, measured under AM 1.5 illumination (100 mWcm⁻²).

Table 4. 2 Photovoltaic properties of ZnSe/CdS type II Core/Shell QDSSCs measured 1 sun illumination.

Samples	J _{sc} (mAcm ⁻²)	V _{oc} (V)	FF	η(%)
ZnSe/CdS	3.49	0.175	46.46	0.28

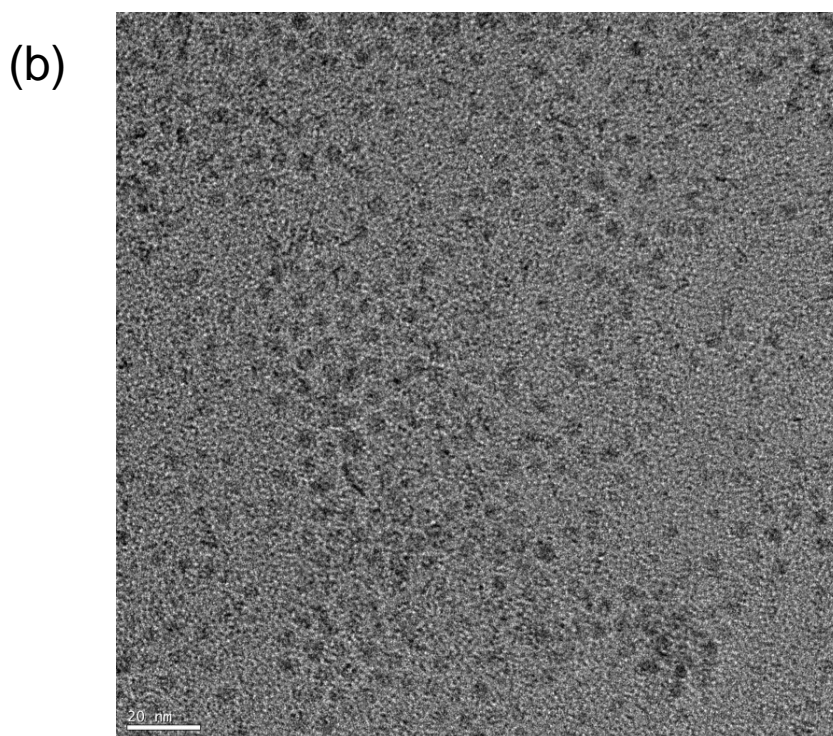
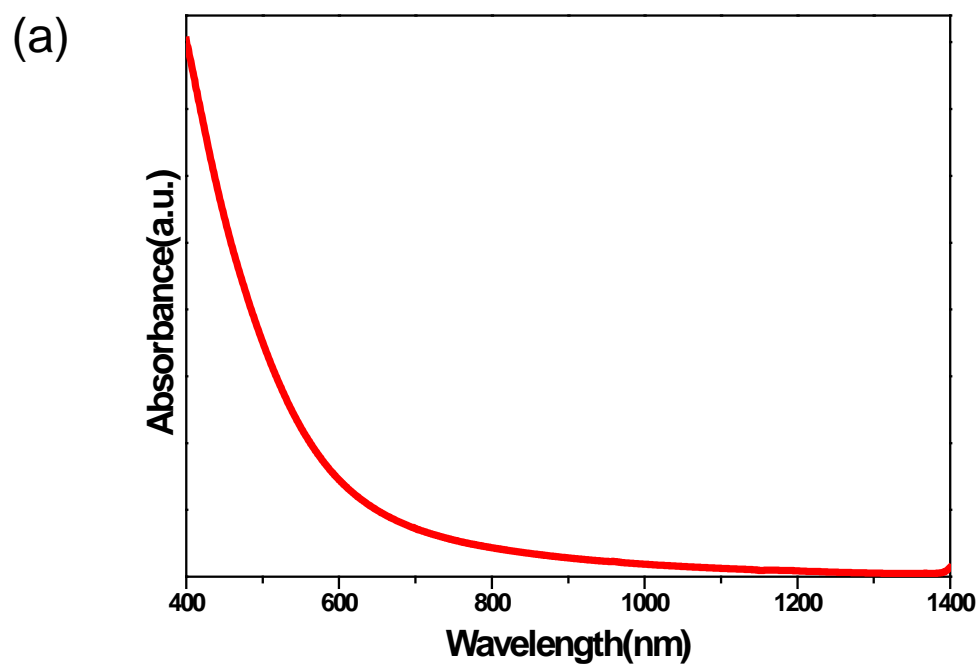


Fig 4. 9 Properties of FeS_2 NCs. (a) UV-Vis-NIR absorption of FeS_2 NCs shows a wide absorption up to 1400nm, (b) TEM image of FeS_2 NCs with an average diameter of 2nm.

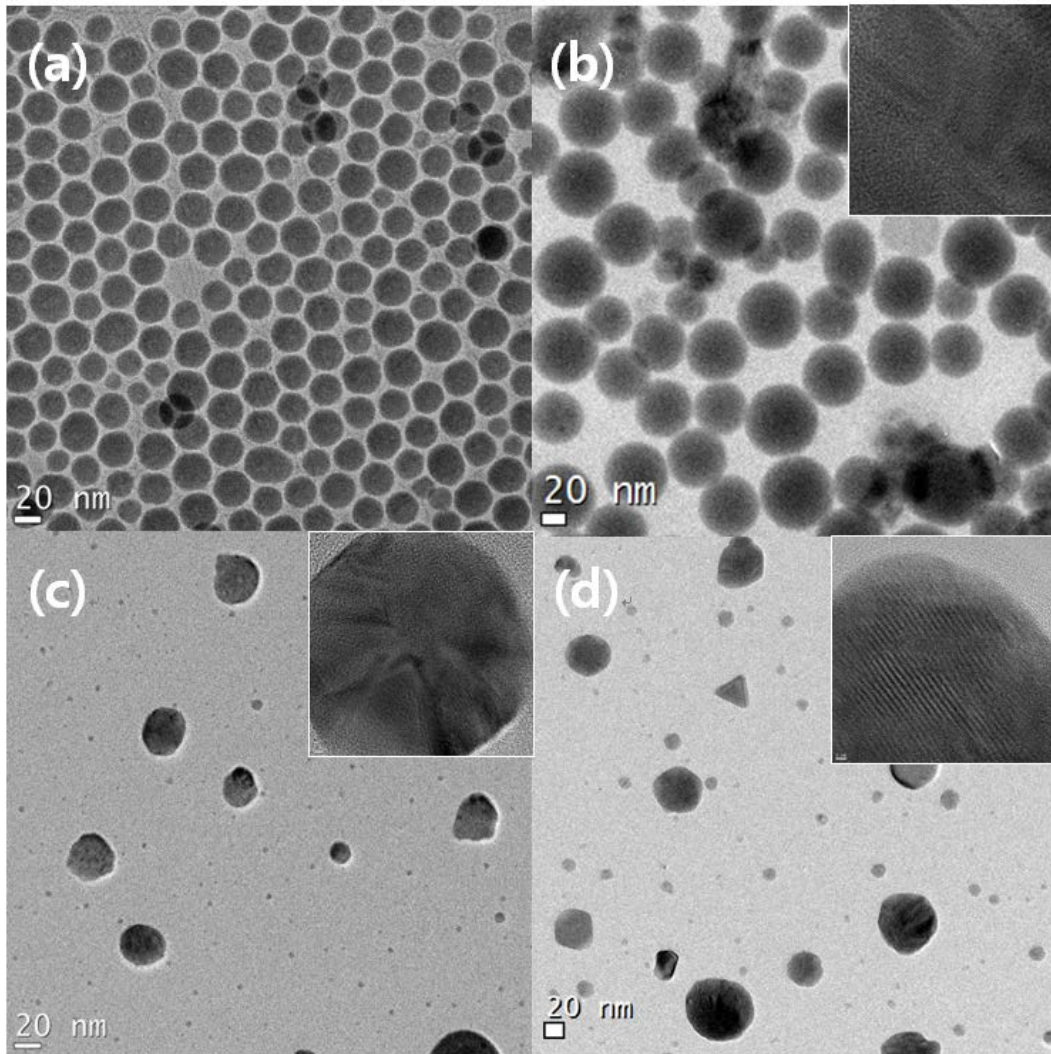


Fig 4. 10 Optical properties of Sb_2S_3 . (a) TEM image of amorphous, orange, Sb_2S_3 nanoparticle with an average diameter of 20nm, (b)(c)(d) TEM image of crystalline Sb_2S_3 NCs after annealing at 200 °C, 250 °C, 300 °C for 1 hour(inset HR-TEM).

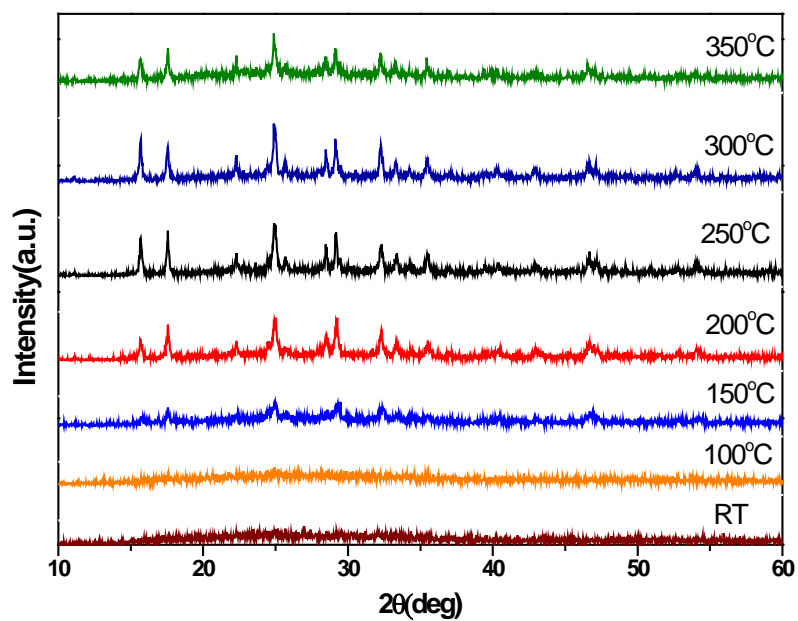


Fig 4. 11 Temperature dependence XRD patterns of Sb_2S_3 films: Sb_2S_3 nanoparticles were deposited to glass substrate and annealed at 100 °C, 150 °C, 200 °C, 300 °C, 350 °C, separately. The phase transition appeared from 150 °C and XRD patterns of samples annealed from 200 °C to 350 °C indicate that samples were crystallized.

5. Conclusion

In conclusion, CdSe QDs, ZnSe/CdS type-II core/shell, Cu₂S QDs were synthesized and their optical and electronic properties were characterized. And nanostructures of Sb₂S₃, FeS₂ were synthesized for further application of QDSSCs. These CdSe QDs and type-II QDs were applied for sensitizers of QDSSCs. The CdSe QDSSCs and ZnSe/CdS type-II core/shell QDSSCs were tested under 1 sun illumination and Cu₂S NCs were used as counter electrode for increasing high catalytic activity and stability. In this study, the solar cell performance depending on the different sensitizer materials for photoanode. In addition, combining Cu₂S NCs counter electrode was performed. The results show that cell performance of $J_{sc}=2.6\text{mA/cm}^{-2}$, 3.496mA/cm^{-2} , $V_{oc}=0.377\text{V}$, 0.179V , $FF=47.2\%$, 46.46% and $\text{efficiency}=0.465\%$, 0.28% in CdSe QDSSC, ZnSe/CdS type-II core/shell QDSSCs separately. Our results showed that ZnSe/CdS type-II QDSSCs exhibited higher short-circuit current density and longer decay lifetime than CdSe QDSSCs. Both the absorption and fluorescence spectra proved the charge separation character of the type-II QDs, which effectively broadened the absorption spectra without a decrease in the conduction band.

요 약 문

Type II 코어셸 나노결정 양자점의 합성과 양자점 감응형 태양전지에 대한 연구

본 연구는 hot injection 방법을 통하여 양자점 태양전지에 응용할 colloidal nanoparticles을 합성하고 폴리설파이드계열의 전해질을 이용하는 양자점 감응형 태양전지가 양극에 적용되는 감광물질에 따라서 어떠한 특성을 내는지 살펴보았다. CdSe와 같은 단일 구조 양자점이 가장 많이 감광물질로 이용되고 있다. 다층구조의 Type-II 코어셸 양자점은 높은 코어에 국한되고 전자는 셸에 국한 되어 전자정공의 효율적인 분리를 가능하게 하여 우수한 전기적 특성을 지닐것으로 생각되었다. 이에 본 연구에서는 Type-II 물질을 합성하여 양자점 감응형 태양전지의 감광물질로 적용하고자 하였으며 ZnSe 양자점을 합성한 후 layer-by-layer growth technique 을 이용하여 CdS 셸을 코어 물질에 쌓았다. 코어에 쌓는 셸의 두께에 따라 양자 점의 크기가 증가함으로써 Absorption Spectra가 장파장으로 이동한 것을 볼 수 있었으며 우수한 전자 이동과 흡수 스펙트럼을 가지기 위하여 3층의 CdS 셸을 쌓았다. Type-II 코어셸 양자점의 전하 분리 특성을 통해 ZnSe/CdS Type-II 코어셸을 활용했을 때 CdSe 보다 높은 J_{sc} 값을 얻을 수 있었다. Time-resolved transient fluorescence spectra를 이용하여 단일구조의 CdSe 보다 다층구조의 ZnSe/CdS Type-II 코어셸이 더 긴 decay time을 가지는 것도 확인 할 수 있었다. 하지만 ZnSe/CdS Type-II QDSSCs가 CdSe QDSSCs보다 낮은 V_{oc} 값을 가져 낮은 효율을 보여주었다. 낮은 V_{oc} 값의 원인으로는 여기된 전자가 전해질에서의 높은 재결합 때문일 것으로 생각한다. 우수한 흡광계수와 적절한 밴드갭을 가져 유망한 감광물질로 기대되는 Sb_2S_3 나노파티클을 hot injection 방법을 통하여 합성하였다. 비정질의 colloidal Sb_2S_3 솔루션을 유리기판 위에 drop casting하여 온도 별로 어닐링을 진행하였다. 그 결과 결정성을 지니는 Sb_2S_3 나노파티클을 TEM을 통해 확인할 수 있었으며 온도가 증가함에 따라 강하게 결정성을 띄었다. 광전자 물질로 촉망 받는 FeS_2 나노결정 또한 hot injection 방법을 통해 합성 하였으며 UV-Vis와 TEM을 통해 특성을 분석 하였다.

References

1. Hodes, G., *Comparison of Dye- and Semiconductor-Sensitized Porous Nanocrystalline Liquid Junction Solar Cells*. Journal of Physical Chemistry C, 2008. **112**(46): p. 17778-17787.
2. Hagfeldt, A., et al., *Dye-Sensitized Solar Cells*. Chemical Reviews, 2010. **110**(11): p. 6595-6663.
3. Chang, C.-H. and Y.-L. Lee, *Chemical bath deposition of CdS quantum dots onto mesoscopic TiO₂ films for application in quantum-dot-sensitized solar cells*. Applied Physics Letters, 2007. **91**(5): p. 053503.
4. Shen, Q., et al., *Effect of ZnS coating on the photovoltaic properties of CdSe quantum dot-sensitized solar cells*. Journal of Applied Physics, 2008. **103**(8): p. 084304.
5. Ning, Z., et al., *Solar cells sensitized with type-II ZnSe-CdS core/shell colloidal quantum dots*. Chem Commun (Camb), 2011. **47**(5): p. 1536-8.
6. Jun, H.K., M.A. Careem, and A.K. Arof, *Quantum dot-sensitized solar cells—perspective and recent developments: A review of Cd chalcogenide quantum dots as sensitizers*. Renewable and Sustainable Energy Reviews, 2013. **22**: p. 148-167.
7. Kim, S., et al., *Novel type-II quantum dots: CDTE/CDSE(core/shell) and CDSE/ZNTE(core/shell) heterostructures*. Abstracts of Papers of the American Chemical Society, 2002. **224**: p. U443-U443.

8. Dimroth, F., et al., *Wafer bonded four-junction GaInP/GaAs//GaInAsP/GaInAs concentrator solar cells with 44.7% efficiency*. Progress in Photovoltaics: Research and Applications, 2014. **22**(3): p. 277-282.
9. Peter, L.M., *Towards sustainable photovoltaics: the search for new materials*. Philos Trans A Math Phys Eng Sci, 2011. **369**(1942): p. 1840-56.
10. Bergmann, R.B., *Crystalline Si thin-film solar cells: a review*. Applied Physics a- Materials Science & Processing, 1999. **69**(2): p. 187-194.
11. Green, M.A., *Crystalline and thin-film silicon solar cells: state of the art and future potential*. Solar Energy, 2003. **74**(3): p. 181-192.
12. Pagliaro, M., R. Ciriminna, and G. Palmisano, *Flexible solar cells*. ChemSusChem, 2008. **1**(11): p. 880-91.
13. Shah, A., *Photovoltaic Technology: The Case for Thin-Film Solar Cells*. Science, 1999. **285**(5428): p. 692-698.
14. Grätzel, M., *Dye-sensitized solar cells*. Journal of Photochemistry and Photobiology C: Photochemistry Reviews, 2003. **4**(2): p. 145-153.
15. Oregan, B. and M. Gratzel, *A LOW-COST, HIGH-EFFICIENCY SOLAR-CELL BASED ON DYE-SENSITIZED COLLOIDAL TiO₂ FILMS*. Nature, 1991. **353**(6346): p. 737-740.
16. Smith, A.M. and S. Nie, *Semiconductor Nanocrystals: Structure, Properties, and Band Gap Engineering*. Accounts of Chemical Research, 2010. **43**(2): p. 190-200.
17. Ruhle, S., M. Shalom, and A. Zaban, *Quantum-dot-sensitized solar cells*.

- Chemphyschem, 2010. **11**(11): p. 2290-304.
18. Pisanic, T.R., 2nd, Y. Zhang, and T.H. Wang, *Quantum dots in diagnostics and detection: principles and paradigms*. Analyst, 2014. **139**(12): p. 2968-81.
 19. Li, J.J., et al., *Large-scale synthesis of nearly monodisperse CdSe/CdS core/shell nanocrystals using air-stable reagents via successive ion layer adsorption and reaction*. Journal of the American Chemical Society, 2003. **125**(41): p. 12567-12575.
 20. Nozik, A.J., *Multiple exciton generation in semiconductor quantum dots*. Chemical Physics Letters, 2008. **457**(1-3): p. 3-11.
 21. Kongkanand, A., et al., *Quantum dot solar cells. Tuning photoresponse through size and shape control of CdSe-TiO₂ architecture*. Journal of the American Chemical Society, 2008. **130**(12): p. 4007-4015.
 22. Peter, L.M., *The Gratzel Cell: Where Next?* Journal of Physical Chemistry Letters, 2011. **2**(15): p. 1861-1867.
 23. Li, L., et al., *Highly efficient CdS quantum dot-sensitized solar cells based on a modified polysulfide electrolyte*. J Am Chem Soc, 2011. **133**(22): p. 8458-60.
 24. Sima, C., C. Grigoriu, and S. Antohe, *Comparison of the dye-sensitized solar cells performances based on transparent conductive ITO and FTO*. Thin Solid Films, 2010. **519**(2): p. 595-597.
 25. Kamat, P.V., *Quantum Dot Solar Cells. The Next Big Thing in Photovoltaics*. The Journal of Physical Chemistry Letters, 2013. **4**(6): p. 908-918.
 26. Xu, X., et al., *Influence of cysteine adsorption on the performance of CdSe quantum*

- dots sensitized solar cells*. *Materials Chemistry and Physics*, 2010. **124**(1): p. 709-712.
27. Margraf, J.T., et al., *Quantum-dot-sensitized solar cells: understanding linker molecules through theory and experiment*. *Langmuir*, 2013. **29**(7): p. 2434-8.
 28. Mora-Sero, I., et al., *Factors determining the photovoltaic performance of a CdSe quantum dot sensitized solar cell: the role of the linker molecule and of the counter electrode*. *Nanotechnology*, 2008. **19**(42): p. 424007.
 29. Wang, Y.-C., et al., *FeS₂ Nanocrystal Ink as a Catalytic Electrode for Dye-Sensitized Solar Cells*. *Angewandte Chemie-International Edition*, 2013. **52**(26): p. 6694-6698.
 30. Lim, C.-S., et al., *Hole-conducting mediator for stable Sb₂S₃-sensitized photoelectrochemical solar cells*. *Journal of Materials Chemistry*, 2012. **22**(3): p. 1107-1111.